Investigating the Atlantic-monsoon teleconnection pathways in PMIP3 Last Millennium Simulations

Arijeet Dutta[1], Rahul Sivankutty[2] and *J M Neena[1]

[1]Indian Institute of Science Education and Research Pune, India
[2]British Antarctic Survey

Manuscript Submitted to Climate Dynamics

***Corresponding Author:**
Dr Neena J Mani
Earth and Climate Science,
Indian Institute of Science Education and Research Pune, India
Email: neena@iiserpune.ac.in

Abstract

The Atlantic multidecadal oscillation (AMO) is considered as one of the major drivers of Indian Summer monsoon (ISM) multidecadal variability, but the exact mechanism of teleconnection remains elusive. AMO can impact the ISM dominantly by two pathways – by generating upper-level circulation and heating responses across Eurasia and via the Pacific through the atmospheric bridge mechanism and associated modulations of Hadley-Walker circulations in the Indo-Pacific. Using the PMIP3 Last millennium (LM) simulations, the current study investigates the AMO-ISM teleconnection in the context of these pathways of interaction. A significant positive correlation is observed between AMO and ISM in five of the eight models. While the models display only limited skill in simulating the upper-level circulation and tropospheric temperature responses involved in the Eurasian pathway, they exhibit better skill in capturing the Pacific SST responses induced by the AMO. Four of the five models capture the AMO modulation of summer North Atlantic Oscillation (SNAO), but major discrepancies are observed in the SNAO downstream responses. CCSM4 and MPI exhibit better skill in simulating the AMO forced upper-level circulation responses across Eurasia, while CSIRO, GISS and MRI-CGCM3 exhibit better skill in simulating the AMO modulation of extra tropical-tropical SST gradient over the Pacific. Reliability of decadal climate predictions of ISM largely depends on the fidelity of current generation global models in simulating the teleconnection mechanisms which modulate the ISM multidecadal variability, and results from the current study helps in highlighting some of the main deficiencies in model simulated teleconnection processes.

Introduction

The boreal summer monsoon serves as the main source of precipitation over the South Asian region and forecasting its variability in the intraseasonal and inter-annual timescales is of great relevance for socio-economic planning and policy making in the South Asian countries. The interannual variability of monsoon is strongly modulated by the low frequency modes of variability in the decadal and longer timescales. Observational records indicate that the seasonal mean Indian Summer monsoon (ISM) exhibits multidecadal variability with a periodicity of ~60 years (Mooley and Parthasarathy 1984; Krishnamurthy and Goswami 2000; Goswami 2006; Zhou et al. 2010) and the seasonal mean ISM rainfall was found to be above the long term mean during the decades 1871–1900 and 1931–1960 and below the long-term mean during 1901–1930 and 1961–1990 (Mooley and Parthasarathy 1984). The multidecadal variability of monsoon is also evident in paleoclimate reconstructions from different parts of the monsoon domain (Burns et al. 2002; Sinha et al. 2007, 2011; Berkelhammer et al. 2010; Goswami et al. 2016). While climate forcing like changes in solar irradiance and volcanic activity are known to modulate the monsoon variability in the multidecadal timescales (e.g. Agnihotri et al. 2002; Bhattacharyya and Narasimha 2005; Bollasina et al. 2011), internal variability associated with low frequency climate modes over the Atlantic and Pacific Oceans also play a major role in modulating ISM multidecadal variability (e.g. Krishnan and Sugi 2003; Zhang and Delworth 2006). The major multidecadal mode observed over the Pacific Ocean, namely the Pacific Decadal Oscillation (PDO) (Mantua et al. 1997) has a periodicity of around 30-50 years (Deser et al. 2010) and it exhibits an inverse relationship with the ISM variability (Krishnan and Sugi 2003; Krishnamurthy and Krishnamurthy 2014; Joshi and Kucharski 2017; Huang et al. 2020). On the other hand, coherent ocean-atmosphere coupled variability over the North Atlantic basin, the Atlantic Multidecadal oscillation (AMO) (Bjerknes 1964; Delworth and Mann 2000; Enfield et al, 2001; Knight et al. 2005), exhibits an in phase relationship with the ISM multidecadal variability. It exhibits a periodicity of about 50-80 years in the instrumental records and in paleoclimate reconstructions (Schlesinger and Ramankutty 1994; Gray et al. 2004; Parker et al. 2007; Tung and Zhou 2013; Naidu et al. 2020).

The AMO has been established as one of the major drivers of the multidecadal variability of ISM during the instrumental period (Zhang and Delworth 2006; Goswami et al. 2006; Lu et al. 2006; Feng & Hu 2008; Joshi and Rai 2015; Krishnamurthy and Krishnamurthy 2015), and the decades of warmer (cooler) than normal SST anomalies over the Atlantic are associated with higher (lower) than normal precipitation over the ISM domain. Paleoclimate studies however brings out diverse interpretations of the AMO-ISM relationship. Independent monsoon reconstructions for the past two millennia based on Dandak cave speleothem (Berkelhammer et al. 2010) and Bay of Bengal sediment cores (Naidu et al. 2020) (Naidu et al. 2020) largely attribute the ISM multidecadal variability to AMO. Feng and Hu (2008) analyzed the proxies of ISM, Atlantic SST and Tibetan heating for the last two millennia and showed that weak monsoon periods correspond to cooler SST conditions over the North Atlantic, but strong monsoon periods do not always accompany warmer conditions over the Atlantic. In another study based on multiple proxy records for the last 500 years, Sankar et al. (2016) showed that the positive relationship between AMO and ISM was not prominent before 1800. While many modeling studies (e.g. Li et al. 2008; Wang et al. 2009; Luo et al. 2011; Malik et al. 2017) corroborate the observed relationship between the AMO and ISM, analysis of a suite of climate model simulations, part of the Coupled Model Intercomparison Project (CMIP) indicate that the AMO-ISM relationship is highly variable among different models (Ting et al. 2011; Luo et al. 2018). In the CMIP5 historical simulations, only ~16% of the models could reproduce a statistically significant relationship between AMO and ISM (Luo et al, 2018). Nevertheless, the current generation climate models are an indispensable tool for making long term climate forecasts. The reliability of decadal climate predictions/projections of monsoon will largely depend on how successful the models are in simulating the different teleconnection mechanisms which modulate the ISM multidecadal variability.

Studies investigating the multidecadal linkages between the Atlantic and the ISM identify three main pathways of teleconnection. In the interannual timescale, the North Atlantic Oscillation (NAO) exerts a downstream impact on the ISM by modulating the surface temperature over Eurasia and the moisture flux by the south westerly winds over the ISM domain (Chang et al. 2001; Srivastava et al. 2002; Roy and Kripalani 2019; Krishnamurthy and Krishnamurthy 2015). Using data from the instrumental period, several studies (Goswami et al 2006; Folland et al. 2008; Peings and Magnusdottir 2014; Krishnamurthy and Krishnamurthy 2015) showed that a positive AMO phase is conducive for frequent occurrence of negative NAO phase over the Atlantic in summer, which in turn leads to strong monsoon conditions over the ISM domain. Atmospheric heating anomalies associated with warm SST anomalies over the north Atlantic can also induce planetary wave responses across Eurasia, which can lead to upper-level circulation anomalies over central Asia can alter the ISM strength through easterly shear modulation (Luo et al. 2011). Dutta and Neena (2022) showed that this mode of teleconnection has a prevalent impact in the multidecadal timescale as well. Several observation/modelling studies also indicate that the AMO influence on the ISM might be mediated by the Pacific (Zhang and Delworth 2007; Kucharski et al. 2016; Sun et al. 2017, 2019). Warming over the Atlantic Ocean can induce a secondary warming over the north Pacific though an atmospheric bridge mechanism. Through circulation responses and atmosphere-ocean feedbacks, this can lead to strong ISM conditions. The extratropical-tropical SST gradient over the north Pacific was found to be a crucial factor in the AMO-ISM teleconnection in CMIP5 model simulations (Luo et al. 2018), as a stronger gradient over the North Pacific signifies an enhanced Walker circulation and a stronger ISM. In this study we explore the AMO-ISM relationship in the Last millennium (LM) simulations by climate models participating in the Paleo climate Modeling Intercomparison Project phase 3 (PMIP3), considering the above discussed teleconnection mechanisms. LM simulations provide a long record of Atlantic and ISM variability and it provides an opportunity to examine the impact of internal climate variability on ISM (Tejavath et al. 2019; Ashok et al. 2022). By examining the AMO-ISM teleconnections during the LM in different model climates, we hope to gain insight on the robustness of the relationship over longer time periods. Understanding how the relationship emerge in different model climates will provide crucial information on the natural variability of the climate modes, and it holds immense value in the context of decadal climate prediction. The study also aims to identify the dominant teleconnection pathways through which the Atlantic influences the ISM.

Data and Methodology

The AMO-ISM teleconnection in the Last Millennial (LM) simulations (850-1850) by eight climate models from the Paleoclimate Model Intercomparison Project phase 3 (PIMP3) (Braconnot et al. 2012) archive are analyzed in the study. The LM simulations were included as a part of the PMIP3 to gain a long-term perspective for detection and attribution studies and to evaluate the models ability in simulating the multidecadal and longer time scale climate variability. The LM simulations were forced with historical reconstructions of total solar irradiance, volcanic aerosols and greenhouse gas concentrations (Schmidt et al. 2012). Topography, vegetation, and ice sheets were maintained as same as the pre-Industrial control conditions. Atmospheric and oceanic fields of monthly resolution from eight PMIP3 coupled global climate model (GCM) simulations were downloaded from the Earth System Grid Federation (ESGF) data servers and https://www.wdc-climate.de/ui/ (see Table 1 for the list of models). As an observational counterpart, only for the purpose of comparing with the known climate features during the instrumental period, mean sea level pressure, air temperature, and wind data from 20th Century reanalysis (1901-2012), Hadley Centre Sea Ice and Sea Surface Temperature data (1901-2012) (HadISST, Rayner et al. 2003), monthly precipitation data from Global Precipitation Climatology Project V2 (GPCP, Adler et al. 2003) (1979-2012) and a long record of all-India mean rainfall data (1871-2012) from IITM were used. All observation and model fields were re-gridded to a 2°×2° uniform grid. Anomalies of different fields were computed as departures from monthly climatology computed over the last 100 years of LM simulation, i.e., from 1750-1850. The overall trend in the LM simulations was removed using least square fit method. To identify the robust multidecadal spectral signature from the long time series, power spectra was computed using the Welch method (Welch 1967). The power spectra were estimated by applying fast Fourier transform (FFT) to 200-year segments with 40% overlap, and then the average spectra were computed. The theoretical red-noise spectrum is estimated from the lag-1 autocorrelation value of the original time series and the 90% significance limit was estimated using the Chi-square test.

To compute the Atlantic Multidecadal variability (AMV) index, the annual mean sea surface temperature (SST) was averaged over the north Atlantic (75°W -5°E, 0-60°N). The global average SST time series was then subtracted from this time series, to remove the influence of other globally uniform climate signals (following Trenberth and Shea 2006). This method of removing the global mean SST signal from the North Atlantic SST variability was found to be useful in bringing out the AMV related signals in climate model simulations (Lyu and Yu 2017). Since our focus is to understand climate variability in the multidecadal timescales, a 30-100 year Lanczos filter (Duchon 1979) was applied to the model AMV time series, while a 30-year low-pass filter was applied to the HadISST based AMV time series. These filtered time series represent the respective AMO indices which were used for further analysis. To calculate the probability distribution of parameters during different AMO phases, we used the gaussian kernel density estimate (Rosenblatt 1956; Parzen 1962). The PDF is given as

$$p_n(x) = \frac{1}{nh}\sum_{i=1}^{n} K(x)\left(\frac{X_i - x}{h}\right)$$

Where n is number of data points, h is smoothing bandwidth and $K(x)$ is the gaussian kernel function given as $\frac{1}{\sqrt{2\pi}}\, e^{\frac{-x^2}{2}}$. Kernel density estimate basically smoothens each data point X_i

into small density bumps and then sum all these small bumps together to obtain the final density estimate.

Results and Discussion

The climatological mean state over the ISM domain was first examined in the LM simulations by the eight GCMs. The June to September (JJAS) mean precipitation averaged over the Last Millennia is shown in Figure 1. While it is not meaningful to estimate the model biases relative to present day observations, the climatological mean (1979-2012) ISM precipitation in the GPCP v2 dataset is shown alongside for easy comparison with present day monsoon features. Earlier studies (Menon et al., 2013; Sengupta & Rajeevan, 2013) have documented the skill of these models in simulating the ISM features in the CMIP5 historical simulations. The main features of the ISM in the LM simulations do not differ much from the monsoon features in the historical simulations (cf: Figure 3, Menon et al., 2013). While models like CCSM4, MPI and MIROC simulate the mean monsoon precipitation pattern with relatively good fidelity, GISS, MRI-CGCM3, HADCM3, BCC and CSIRO underestimate the precipitation over Indian landmass, and this has been recognized as a fundamental bias in climate models (Dai 2006; Sabeerali et al. 2015). Power spectral analysis of all-India mean ISM rainfall data (1871-2012) brings out a 50–100-year multidecadal signal along with a higher frequency multidecadal mode around 30 year (Figure 2). In the LM simulations the spectra was calculated using area averaged ISM rainfall over the domain (60°-100°E, 5°-27°N). A similar distribution of spectral power is observed in the LM simulations by BCC, CCSM4 and MRI-CGCM3, while in other models a broad spectral range of 10-60 year or 10-100 year is observed.

Climatological representation of seasonal mean monsoon winds at 850hPa pressure level and near surface air temperature (10m) in the LM simulations are shown in Figure 3. As an observational counterpart from the instrumental period, JJAS mean fields from the 20th Century reanalysis are shown alongside. The simulation of these dynamic and thermodynamic fields gives useful information about the models' ability in simulating the large-scale monsoon system. While there are significant biases in the model simulated monsoon precipitation, most models simulate the summertime heating and low-level winds over the ISM landmass with reasonably good skill, as in the case of historical simulations (Sengupta and Rajeevan 2013). The models capture the high surface temperature conditions over the Thar desert region and adjoining areas over northwest India and the warm conditions over the northern Indian Ocean. Most models also simulate the cross equatorial low level flow from the Somalia coast towards the Indian subcontinent, albeit some small differences in the strength and extent of the low-level Jetstream (LLJ). The vertically averaged free tropospheric temperature over the monsoon domain measures the monsoon diabatic heating and hence is a useful index for the strength of ISM (Goswami and Xavier 2005). The climatological mean patterns of upper level (200 hPa) circulation and free tropospheric temperature (averaged from 500-200 hPa) over the ISM domain are shown in Figure 4. The co-location of the upper tropospheric anticyclones and the maximum heating zone is evident in the 20th Century reanalysis. The seasonal mean free tropospheric temperature over the ISM domain is underestimated in most models relative to 20th century observations, but the broad features of the upper-level circulation including the upper tropospheric anticyclone and tropical easterly jet are simulated by most of the models. Most of the models also capture the north south gradient in tropospheric temperature over the ISM domain. BCC, GISS and MPI have a relatively poor representation of the monsoon core zone of heating in terms of both intensity and spatial extent. From the analysis of the mean monsoon features, it can be surmised that even though the models have some weaknesses in the simulation of monsoon precipitation, they mostly capture the heating and mean circulation features associated with the large-scale monsoon system.

To delineate how the multidecadal variability over the Atlantic Ocean is captured in the LM simulations, we examined the power spectra of the basin averaged AMV index (Figure 5). The periodicity of AMO derived from observations and paleoclimate reconstructions fall in the 50-80 year timescale (Schlesinger and Ramankutty 1994; Gray et al. 2004; Parker et al. 2007; Tung and Zhou 2013). A broad range of spectral power is observed in the 30–100-year timescale in most of the models. Significant spectral power in the 10–30-year timescale is also present in some models such as, CCSM4, MPI, BCC and GISS. Earlier studies which examined the AMV in the historical and pre industrial simulations by CMIP models (Ting et al. 2011; Peings et al. 2016; Ratna et al. 2019) have also reported a wide range of spectral power in the multidecadal timescale over the Atlantic. Both observations and climate models indicate that apart from the basin wide mode of multidecadal warming/cooling which is known as the Atlantic Multidecadal Oscillations (AMO), a tri-pole pattern of variability with cold SST anomalies over western Atlantic between 10°N-40°N sandwiched between warm SST anomalies to the east of Newfoundland, and over the tropical eastern Atlantic, is also dominant over the Atlantic (Wu and Liu 2005; Fan and Schneider 2012; Lin et al. 2019). Since the focus of the present study is to understand the multidecadal scale influence of the Atlantic on the ISM, a common 30–100-year band is chosen as representative of AMO in the models and the

30-100 year filtered AMV timeseries is used as the AMO index in the remaining analysis. The spatial structure of the model simulated AMO was examined by compositing 30–100-year filtered SST anomalies for positive and negative AMO phases (Figure 6). The positive (negative) phases of AMO were identified as when the normalized AMO index is greater than 1.0 (less than -1.0) standard deviation. In most models the basin wide warming/cooling signature is evident over the North Atlantic, while in some models like BCC, CSIRO, and MRI-CGCM3 the warm/cold SST anomalies are concentrated over the eastern part of the Atlantic basin. Warm SST anomalies over the north Pacific is evident in the positive AMO phase composites of many models, but the response is diverse among the different models. While positive SST anomalies are observed over most part of the north Pacific in CCSM4 and GISS, positive SST anomalies restricted to the western Pacific domain are observed in BCC, MIROC, HADCM3, MPI, MRI-CGCM3 and CSIRO simulations. Negative SST anomalies over tropical eastern Pacific are simulated in most models except CCSM4 and GISS. In these two models, the Pacific exhibits basin wide warming during positive AMO phase and basin wide cooling during negative AMO phase. It is interesting to note that the SST anomalies over the Indian ocean are in tandem with the SST anomalies over tropical central pacific, during positive/negative AMO phases.

Next, we explore the AMO-ISM relationship in the LM simulations and examine the different teleconnection pathways through which the AMO influences the ISM variability. The correlation between the AMO index and 30-100 year filtered rainfall averaged over the ISM domain (60°E-100°E, 5°N-27°N) during the LM are shown in Table 2. A significant (90% confidence level) positive correlation is observed for the models CCSM4, MRI-CGCM3, CSIRO, HADCM3 and BCC, while for MIROC, GISS and MPI, the correlation is negative or insignificant. On the other hand, Luo et al. (2018) reported a positive correlation between AMO and ISM rainfall in all models except MIROC and HADCM3 in the CMIP5 historical simulations. Considering the biases in the simulation of mean monsoon precipitation, the AMO-ISM relationship in the LM simulations were also explored using a TT gradient based index (Goswami and Xavier 2005) and a zonal wind shear based index (Webster and Yang 1992) for the ISM. The meridional gradient of TT anomalies between the equatorial Indian ocean and the northern land mass plays a major role in maintaining the monsoon circulation and can be considered as an indicator of ISM strength (Goswami and Xavier 2005; Xavier et al. 2007). The TT gradient over the ISM domain was calculated as the difference in vertically averaged TT between a north box (50°E-100°E, 15°N-35°N) over Indian land region and a south box (50°E-100°E, 15°S-5°N) over the Indian Ocean. A significant positive correlation is observed between 30-100 year filtered TT gradient over the ISM domain and the AMO index in the models CCSM4, CSIRO, MRI-CGCM3, MPI and GISS. The correlation is not significant for BCC and HADCM3 and negative in the case of MIROC. The LLJ and the upper-level tropical easterly jet together generates a strong wind shear over the monsoon domain which gives a measure of the strength of the monsoon circulation. The zonal wind shear index is defined as the vertical shear of zonal wind averaged over the region 0°-20°N, 40°-110°E. The wind shear-based index also exhibits a significant correlation with the AMO in all the models except MIROC, BCC and HADCM3. It implies that the multidecadal variability of the circulation and TT over the ISM domain in five of the eight models are largely related with the Atlantic multidecadal variability. In the remaining part of the manuscript, we analyse how each of the proposed teleconnection processes are represented in these five models and explore how it impacts the AMO-ISM relationship.

Modulation of surface temperature and TT over Eurasia is an important factor in the AMO-ISM teleconnection, and a positive (negative) AMO phase is known to be associated with warm tropospheric temperature anomalies over Eurasia and Tibet (Goswami et al. 2006). 30-100 year filtered tropospheric temperature (TT) anomalies (averaged from 500hPa to 200hPa) composited for positive AMO years are shown in Figure 7. In the 20th Century reanalysis, during AMO positive phase, maximum positive TT anomalies are observed over the South Asian region, extending from the Mediterranean to the East Asian monsoon domain. All the models simulate an extended band of warm TT anomalies over the South Asian region during positive AMO phase. The TT modulation may happen due to different teleconnection effects. The AMO can induce strong upper tropospheric circulation responses across Eurasia and such teleconnection patterns are associated with significant tropospheric temperature anomalies (Lin et al. 2016; Wu et al. 2016; Sandeep et al. 2022). Barotropic instability over the jet exit region over the north Atlantic gives rise to a quasi-stationary Rossby wave trains which can induce positive geopotential height anomalies over the South Asian high region. An enhanced South Asian high would lead to increased low-level convergence and an amplified meridional TT gradient over the ISM domain (Zhang and Delworth 2006; Luo et al. 2011; Li et al. 2008; Wang et al. 2009). 30-100 year filtered upper level (200hPa) geopotential height anomalies were composited for the positive AMO phase to bring out the upper-level teleconnection pattern associated with the AMO (Figure 8). While an arching teleconnection pattern extending from the Atlantic to central Asian region with alternating positive and negative geopotential height anomalies is evident in the 20th century reanalysis, the model simulated teleconnection patterns are widely different from the observations. Although CCSM4 and MPI LM simulations capture the arching wave train pattern, there are differences in the spatial scale of the geopotential height anomalies and the anomalies are negative over the South Asian domain. Thus, the upper-level wave responses associated with the AMO are not well represented in the models and they may not be responsible for inducing positive TT anomalies over the ISM domain.

The AMO can also impact the ISM via modulating the interannual mode over the Atlantic - the summer NAO (SNAO). It is characterized by an oscillation of the meridional pressure gradient between the Arctic and the subtropical Atlantic and is known to impact the global climate and the ISM. Studies (Baines and Folland 2007; Peings and Magnusdottir 2014; Roy and Kripalani 2019) indicate that a positive (negative) AMO phase would favour a greater number of SNAO negative (positive) events, which in turn would give rise to positive (negative) TT anomalies over Eurasia and in turn affect the meridional TT gradient over the ISM domain. The wind anomalies associated with negative SNAO extending from the Sahel to the western Arabian sea would enhance the south westerly monsoon flow and increase the moisture flux towards the Indian subcontinent, favoring a strong monsoon (Krishnamurthy and Krishnamurthy 2015). Empirical orthogonal function (EOF) analysis of summer time (July-August) mean sea level pressure (SLP) anomalies over the north Atlantic (70°W-50°E, 25°N-70°N) (Folland et al. 2008) is used to extract the summer SNAO dipole structure in the 20th Century reanalysis and the LM simulations (Figure 9). In all the models, the first EOF mode of SLP captures the north south dipole structure associated with SNAO, and the corresponding principal component time series is considered as the representative SNAO index for further analysis. The SNAO pattern is northeastward shifted compared to its winter counterpart, with the southern node observed over northwest Europe (Hurrell et al. 2003; Folland et al. 2009) . However, in the LM simulations, the shifted SNAO pattern is captured only by CCSM4 and MPI. Wang et al (2017) examined the NAO patterns in the CMIP5 historical simulations and reported a wide discrepancy in the locations of NAO high and low pressure centers in the model simulations. They also reported that most of the CMIP5 models tend to underestimate the multidecadal variability of NAO. We find that the multidecadal variability of NAO is underestimated in most models. However, as in observations, the multidecadal (30-100 year) variability of SNAO is found to be negatively correlated with the AMO in all the model simulations except CCSM4 (Table 3). We further examined the frequency of occurrence of positive and negative phases of SNAO during positive and negative AMO phases (Figure 10). SNAO positive and negative phases were identified as when the SNAO index is greater than/less than ±1 standard deviation. In CCSM4 AMO positive phase favors more NAO positive states and vice versa, while in the other four models - CSIRO, MPI, MRI-CGCM3, and GISS, relatively more number of NAO positive states are observed during AMO negative phase, consistent with the observations. On the other hand, the TT anomalies regressed on to the negative SNAO index (Figure 11) brings out a downstream response quite different from observations. While a negative SNAO phase in observations is associated with positive TT responses over Eurasia, in all the models, except MPI, the TT response is negative over Eurasia. Moderate positive TT responses are observed over northern and central Europe in GISS and MRI-CGCM3 simulations but largely the TT responses over the ISM domain are negative in all the models. Similar TT responses are observed in the multidecadal timescale as well (Figure not shown). As the AMO modulation of the SNAO variability in CCSM4 is opposite of that in observations, a positive AMO phase may be conducive for positive SNAO in the model, and it can induce positive downstream TT responses over Eurasia and the ISM domain. On the other hand, in the case of the other four models, the multidecadal modulation of interannual SNAO variability is consistent with observations, but the discrepancies in the downstream responses associated with the SNAO makes this mode of teleconnection to be misrepresented in the models.

The AMO can also modulate the TT gradient over the ISM domain by influencing the SST over the Indian and Pacific Ocean domains. The Southern Indian Ocean SST response of relatively cooler SST anomalies during positive AMO and warmer SST anomalies during negative AMO is simulated by four out of five models - CSIRO, CCSM4, MPI and MRI-CGCM3 (Figure 6). This favors a positive TT gradient over the ISM domain and hence a stronger monsoon. Several studies have shown that the AMO exerts a significant impact on the Pacific variability (Zhang and Delworth 2007; Sun et al. 2017; Gong et al. 2020; Johnson et al. 2020) which affects the ISM. The key features of the observed AMO induced Pacific SST response include warm anomalies over most part of north Pacific (Sun et al, 2017; Gong et al. 2019) and cold anomalies over equatorial eastern Pacific (Kucharski et al. 2016; Johnson et al. 2020) . The SST response is very similar to the PDO and in fact studies have shown that part of the PDO variability may be forced by the AMO (Zhang and Delworth 2007; Johnson et al. 2020; Yang et al. 2020) . The SST response over the Pacific can have a strong impact on the ISM (Feudale and Kucharski 2013; Krishnamurthy and Krishnamurthy 2014; Joshi and

Kucharski 2017; Luo et al. 2018) through modulation of the Walker circulation (Krishnamurthy and Goswami, 2000). While the positive AMO phase is found to be associated with positive SST anomalies over most part of the north Pacific in CCSM4 and GISS, the positive SST anomalies are mostly restricted to the western Pacific domain in the other three models (Figure 6). CCSM4 and GISS fail to simulate the negative SST response observed over tropical eastern Pacific.

Warm SST anomalies over subtropical and extratropical north Pacific are considered to be a response of the Atlantic-Pacific atmospheric bridge mechanism. Upper-level divergence over the Atlantic and convergence and descending motion over northern Pacific, combined with ocean-atmosphere coupled feedbacks can result in warm SST anomalies over subtropical north Pacific (Sun et al. 2017; Gong et al. 2019). Cool SST anomalies over equatorial eastern Pacific during warm AMO phase are thought to be a resultant of anomalous zonal circulation triggered by warm tropical Atlantic. Low level convergence and ascending motion over tropical Atlantic causes large scale subsidence over equatorial eastern Pacific. Resulting high sea level pressure anomalies drive more easterly winds and upwelling and hence cooling over the region (Kucharski et al. 2016). Warming over subtropical north Pacific and cooling over eastern equatorial Pacific leads to a strong extratropical-tropical SST gradient. Positive (negative) phase of AMO induces a positive (negative) extratropical-tropical SST gradient between the extratropical and tropical Pacific. Such SST gradient impacts the ISM through modulation of Hadley-Walker circulation anomalies. Analysing the historical simulations by 22 coupled models that were part of the CMIP5, Luo et al. (2018), showed that models which captured the positive AMO-ISM relationship also successfully simulated the strong extratropical-tropical SST gradient over the Pacific domain. The gradient was calculated between an extratropical Pacific box (25°N–45°N, 150°E–140°W) and tropical eastern Pacific box (15°S–15°N, 180°E–95°W) (following Luo et al. 2018) using 30-100 year filtered SST anomalies. A positive correlation is observed between the Pacific SST gradient and the AMO in all the models (Table 3), with the strongest correlation exhibited by CSIRO, MRI-CGCM3 and GISS models. The probability distribution of the extratropical-tropical SST gradient over the Pacific during positive and negative AMO phases was further examined (Figure 12). In CSIRO, MRI-CGCM3 and GISS, it is evident that a positive AMO phase favors a stronger positive SST gradient over the Pacific, while the separation is not very distinct in the other models. The Pacific SST distribution can impact the ISM, mainly through the modulation of Walker circulation. The Pacific impact on ISM via the Walker circulation in the PMIP3 LM simulations has been reported by Tejavath et al. (2019). 200 hPa velocity potential anomalies composited for periods of strong positive extra tropical-tropical SST gradient over the Pacific (Figure 13) brings out this aspect of the teleconnection. An enhanced Walker circulation is evident in all the models, but it is more westward shifted. While in the 20th century reanalysis we observe upper-level convergence over eastern Pacific and upper level divergence over Western Pacific and ISM domain, all the models exhibit upper level convergence anomalies all over the Pacific domain and upper level divergence prevail over the ISM domain. Nevertheless, the circulation responses to the positive extratropical-tropical SST gradient over the Pacific help in strengthening the monsoon circulation in all the models.

Conclusions

In this study, the observed AMO-ISM relationship is investigated in the Paleoclimate Model Intercomparison Project phase 3 (PMIP3) last millennium (LM) simulations by eight climate models. The LM simulations are useful for gaining a better understanding of the models' ability in simulating the multidecadal and longer time scale climate variability. The model simulated ISM precipitation, circulation and temperature fields were examined, and it was observed that the LM mean monsoon features are very similar to the monsoon features in the historical simulations. While there are some fundamental biases in the simulation of monsoon precipitation by many models, the mean monsoon circulation and heating associated with the large-scale monsoon system are well simulated by most of the models. Similar to the historical and preindustrial simulations by CMIP models, the LM simulations also bring out a broad range of spectral power in the multidecadal timescale over the Atlantic. The AMO in the LM simulations has a periodicity of 30-100 years and capture the basin wide warming signal over the North Atlantic in most models, while in some models like BCC, CSIRO, and MRI-CGCM3 the warm SST anomalies are concentrated over the eastern part of the Atlantic basin. While a consistent positive correlation is not observed between AMO and ISM rainfall in many models, a significant positive correlation is observed between tropospheric temperature based and wind shear-based monsoon indices and the AMO in five out of the eight models - CCSM4, CSIRO, MRI-CGCM3, MPI and GISS. The AMO-ISM relationship in these five models is further explored based on proposed pathways of teleconnection.

Broadly two pathways of AMO-ISM teleconnection are examined, 1) the Eurasian pathway: AMO modulating the monsoon via modulation of tropospheric temperature anomalies over Eurasia and 2) the Pacific pathway: AMO modulating the monsoon via the Atlantic - Pacific atmospheric bridge and associated SST and circulation responses over the Pacific domain. Barotropic instability over the north Atlantic can give rise to upper tropospheric quasi-stationary Rossby wave trains which induce geopotential height anomalies over the South Asian high region and in turn affect the low-level convergence and TT gradient over the monsoon domain. While an arching teleconnection pattern extending from the Atlantic to central Asia is evident in the 20th century reanalysis, none of the models are able to capture such a mode of teleconnection in the LM simulations. CCSM4 and MPI models are found to simulate the arching wave train pattern with relatively better fidelity. In the case of atmospheric teleconnections driven by oceanic forcing, proper simulation of upper atmospheric downstream responses largely depend on the strength and extent of the oceanic forcing. Inter-model differences in the AMO induced upper-level teleconnection pattern hence may be related to the differences in the spatial extent and strength of AMO SST anomalies in the simulations. The TT modulation over Eurasia via the interannual SNAO mode was also explored. A positive AMO phase is known to be conducive for frequent occurrence of negative SNAO phase over the Atlantic, which can have downstream impact on the TT anomalies over Eurasia which is conducive for the ISM. Except CCSM4, in all the other four model simulations, a positive phase AMO is found to favor more SNAO negative states, and the multidecadal SNAO variability is negatively correlated with the AMO, consistent with observations. However, the downstream TT response is quite the opposite of what is expected from observations. While a negative SNAO phase induces positive TT anomalies over the ISM domain in 20th century reanalysis, in all the models a negative SNAO induces negative TT anomalies over the ISM domain. The discrepancies in the model simulated downstream responses associated with SNAO makes this mode of AMO-ISM teleconnection invalid in four of the five models. In CCSM4 however, this mode of teleconnection seems feasible mainly because the AMO bears a positive correlation with the SNAO multidecadal variability.

An important aspect of the Pacific pathway of AMO-ISM teleconnection are the Pacific SST responses induced by the AMO. Positive anomalies in the North pacific and negative SST anomalies in the equatorial eastern Pacific are the signature responses observed over the Pacific in the 20th century reanalysis. While a similar response is observed in MRI-CGCM3, MPI and CSIRO simulations, a positive AMO phase is found to be associated with basin wide positive SST anomalies in CCSM4 and GISS. A strong positive correlation is observed between the Pacific SST gradient and the AMO in all the models, with the strongest correlation exhibited by CSIRO, MRI-CGCM3 and GISS models. Consistent with earlier studies, the Pacific gradient is also accompanied by an enhanced Walker circulation with strong upper-level convergence over the Pacific and divergence over ISM domain. Although there are discrepancies in the finer aspects of teleconnection responses in all the models, some models perform better relative to others in simulating one pathway of teleconnection over the other. While CCSM4 and MPI exhibit better skill in simulating the interannual SNAO mode and the upper-level circulation responses to AMO SST anomalies, these models, CCSM4 in particular, have some major limitation in simulating the AMO forced SST response over the Pacific. The lowest correlation between AMO and the extratropical-tropical SST gradient over the Pacific is observed for CCSM4 and MPI. On the other hand, CSIRO, GISS and MRI-CGCM3 captures the AMO modulation of Pacific SST gradients more realistically. While more detailed analysis is required to understand the nuances of such teleconnection pathways, the Pacific pathway emerges as a better represented teleconnection pathway for AMO-ISM interactions in climate models. Even when multiple teleconnection pathways and their complex interactions might be at play in the observed AMO-ISM co-variability in the current climate state, most of which still remains unknown, it is intriguing to think about the possible teleconnection pathways that might exist in different climates or different model climates. If different model climates may be treated as possible realizations of our climate system, untangling the teleconnection processes in these model climates could be a useful way for assessing the internal variability of the climate system.

Acknowledgments

AD acknowledges the INSPIRE research fellowship from Department of Science and Technology, Government of India, for funding his doctoral research work. NJM acknowledges the DST Climate Change grant for funding her research and IISER Pune for the infrastructure and support. RS acknowledges the British Antarctic Survey.

References

Adler RF, Huffman GJ, Chang A, et al (2003) The version-2 global precipitation climatology project (GPCP) monthly precipitation analysis (1979-present). J Hydrometeorol 4:. https://doi.org/10.1175/1525-7541(2003)004<1147:TVGPCP>2.0.CO;2

Agnihotri R, Dutta K, Bhushan R, Somayajulu BLK (2002) Evidence for solar forcing on the

Indian monsoon during the last millennium. Earth Planet Sci Lett 198:. https://doi.org/10.1016/S0012-821X(02)00530-7

Ashok K, Soraisam B, Tejavath CT, Cubasch U (2022) Summer monsoon over northeastern India during the last millennium. Int J Climatol 42:. https://doi.org/10.1002/joc.7332

B Ratna S, J Osborn T, Joshi M, et al (2019) Identifying teleconnections and multidecadal variability of East Asian surface temperature during the last millennium in CMIP5 simulations. Clim Past 15:. https://doi.org/10.5194/cp-15-1825-2019

Baines PG, Folland CK (2007) Evidence for a rapid global climate shift across the late 1960s. J Clim 20:. https://doi.org/10.1175/JCLI4177.1

Berkelhammer M, Sinha A, Mudelsee M, et al (2010) Persistent multidecadal power of the Indian Summer Monsoon. Earth Planet Sci Lett 290:. https://doi.org/10.1016/j.epsl.2009.12.017

Bhattacharyya S, Narasimha R (2005) Possible association between Indian monsoon rainfall and solar activity. Geophys Res Lett 32:. https://doi.org/10.1029/2004GL021044

Bjerknes J (1964) Atlantic Air-Sea Interaction. In: Landsberg HE, Van Mieghem JBT-A in G (eds). Elsevier, pp 1–82

Bollasina MA, Ming Y, Ramaswamy V (2011) Anthropogenic aerosols and the weakening of the south asian summer monsoon. Science (80-) 334:. https://doi.org/10.1126/science.1204994

Braconnot P, Harrison SP, Kageyama M, et al (2012) Evaluation of climate models using palaeoclimatic data. Nat. Clim. Chang. 2

Burns SJ, Fleitmann D, Mudelsee M, et al (2002) A 780-year annually resolved record of Indian Ocean monsoon precipitation from a speleothem from south Oman. J Geophys Res Atmos 107:. https://doi.org/10.1029/2001JD001281

Chang CP, Harr P, Ju J (2001) Possible roles of atlantic circulation on the weakening Indian monsoon rainfall-ENSO relationship. J Clim 14:2376–2380. https://doi.org/10.1175/1520-0442(2001)014<2376:PROACO>2.0.CO;2

Dai A (2006) Precipitation characteristics in eighteen coupled climate models. J Clim 19:. https://doi.org/10.1175/JCLI3884.1

Delworth TL, Mann ME (2000) Observed and simulated multidecadal variability in the Northern Hemisphere. Clim Dyn 16:. https://doi.org/10.1007/s003820000075

Deser C, Alexander MA, Xie SP, Phillips AS (2010) Sea surface temperature variability: Patterns and mechanisms. Ann Rev Mar Sci 2:. https://doi.org/10.1146/annurev-marine-120408-151453

Duchon CE (1979) Lanczos Filtering in One and Two Dimensions. J Appl Meteorol 18:1016–1022. https://doi.org/10.1175/1520-0450(1979)018<1016:LFIOAT>2.0.CO;2

Dutta A, Neena JM (2022) Exploring the circum-global teleconnection—Indian summer monsoon interactions in the interannual and multidecadal timescales. Front Earth Sci 10:

Enfield DB, Mestas-Nuñez AM, Trimble PJ (2001) The Atlantic multidecadal oscillation and its relation to rainfall and river flows in the continental U.S. Geophys Res Lett 28:. https://doi.org/10.1029/2000GL012745

Fan M, Schneider EK (2012) Observed decadal North Atlantic tripole SST variability. Part I: Weather noise forcing and coupled response. J Atmos Sci 69:35–50. https://doi.org/10.1175/JAS-D-11-018.1

Feng S, Hu Q (2008) How the North Atlantic Multidecadal Oscillation may have influenced the Indian summer monsoon during the past two millennia. Geophys Res Lett 35:1–5. https://doi.org/10.1029/2007GL032484

Feudale L, Kucharski F (2013) A common mode of variability of African and Indian monsoon rainfall at decadal timescale. Clim Dyn 41:. https://doi.org/10.1007/s00382-013-1827-4

Folland CK, Knight J, Linderholm HW, et al (2009) The summer North Atlantic oscillation: Past, present, and future. J Clim 22:1082–1103. https://doi.org/10.1175/2008JCLI2459.1

Folland CK, Linderholm HW, Fereday D, et al (2008) The Summer North Atlantic Oscillation: Past, Present, and Future. J Clim 22:1082–1103. https://doi.org/10.1175/2008jcli2459.1

Gong Z, Sun C, Li J, et al (2020) An inter-basin teleconnection from the North Atlantic to the subarctic North Pacific at multidecadal time scales. Clim Dyn 54:. https://doi.org/10.1007/s00382-019-05031-5

Goswami BN (2006) The Asian monsoon: Interdecadal variability. In: The Asian Monsoon. Springer Berlin Heidelberg, Berlin, Heidelberg, pp 295–327

Goswami BN, Kripalani RH, Borgaonkar HP, Preethi B (2016) Multi-Decadal Variability in Indian Summer Monsoon Rainfall Using Proxy Data. In: World Scientific Series on Asia-Pacific Weather and Climate

Goswami BN, Madhusoodanan MS, Neema CP, Sengupta D (2006) A physical mechanism for North Atlantic SST influence on the Indian summer monsoon. Geophys Res Lett 33:1–4. https://doi.org/10.1029/2005GL024803

Goswami BN, Xavier PK (2005) ENSO control on the south Asian monsoon through the length of the rainy season. Geophys Res Lett 32:. https://doi.org/10.1029/2005GL023216

Gray ST, Graumlich LJ, Betancourt JL, Pederson GT (2004) A tree-ring based reconstruction of the Atlantic Multidecadal Oscillation since 1567 A.D. Geophys Res Lett 31:2–5. https://doi.org/10.1029/2004GL019932

Huang X, Zhou T, Turner A, et al (2020) The recent decline and recovery of Indian summer monsoon rainfall: Relative roles of external forcing and internal variability. J Clim 33:. https://doi.org/10.1175/JCLI-D-19-0833.1

Hurrell JW, Kushnir Y, Ottersen G, Visbeck M (2003) An overview of the north atlantic oscillation. In: Geophysical Monograph Series

Johnson ZF, Chikamoto Y, Wang SYS, et al (2020) Pacific decadal oscillation remotely forced by the equatorial Pacific and the Atlantic Oceans. Clim Dyn 55:. https://doi.org/10.1007/s00382-020-05295-2

Joshi MK, Kucharski F (2017) Impact of Interdecadal Pacific Oscillation on Indian summer monsoon rainfall: an assessment from CMIP5 climate models. Clim Dyn 48:. https://doi.org/10.1007/s00382-016-3210-8

Joshi MK, Rai A (2015) Combined interplay of the Atlantic multidecadal oscillation and the interdecadal Pacific oscillation on rainfall and its extremes over Indian subcontinent. Clim Dyn 44:. https://doi.org/10.1007/s00382-014-2333-z

Knight JR, Allan RJ, Folland CK, et al (2005) A signature of persistent natural thermohaline circulation cycles in observed climate. Geophys Res Lett 32:1–4. https://doi.org/10.1029/2005GL024233

Krishnamurthy L, Krishnamurthy V (2014) Influence of PDO on South Asian summer monsoon and monsoon-ENSO relation. Clim Dyn 42:. https://doi.org/10.1007/s00382-013-1856-z

Krishnamurthy L, Krishnamurthy V (2016) Teleconnections of Indian monsoon rainfall with AMO and Atlantic tripole. Clim Dyn 46:2269–2285. https://doi.org/10.1007/s00382-015-2701-3

Krishnamurthy V, Goswami BN (2000) Indian monsoon-ENSO relationship on interdecadal timescale. J Clim 13:. https://doi.org/10.1175/1520-0442(2000)013<0579:IMEROI>2.0.CO;2

Krishnan R, Sugi M (2003) Pacific decadal oscillation and variability of the Indian summer monsoon rainfall. Clim Dyn 21:. https://doi.org/10.1007/s00382-003-0330-8

Kucharski F, Parvin A, Rodriguez-Fonseca B, et al (2016) The teleconnection of the tropical Atlantic to Indo-Pacific sea surface temperatures on inter-annual to centennial time scales: A review of recent findings. Atmosphere (Basel) 7:1–20. https://doi.org/10.3390/atmos7020029

Li S, Perlwitz J, Quan X, Hoerling MP (2008) Modelling the influence of North Atlantic multidecadal warmth on the Indian summer rainfall. Geophys Res Lett 35:1–6. https://doi.org/10.1029/2007GL032901

Lin JS, Wu B, Zhou TJ (2016) Is the interdecadal circumglobal teleconnection pattern excited by the Atlantic multidecadal Oscillation? Atmos Ocean Sci Lett 9:451–457. https://doi.org/10.1080/16742834.2016.1233800

Lin P, Yu Z, Lü J, et al (2019) Two regimes of Atlantic multidecadal oscillation: cross-basin dependent or Atlantic-intrinsic. Sci Bull 64:. https://doi.org/10.1016/j.scib.2018.12.027

Lu R, Dong B, Ding H (2006) Impact of the Atlantic Multidecadal Oscillation on the Asian summer monsoon. Geophys Res Lett 33:. https://doi.org/10.1029/2006GL027655

Luo F, Li S, Furevik T (2011) The connection between the Atlantic Multidecadal Oscillation and the Indian Summer Monsoon in Bergen Climate Model Version 2.0. J Geophys Res Atmos 116:1–9. https://doi.org/10.1029/2011JD015848

Luo F, Li S, Gao Y, et al (2018) The connection between the Atlantic multidecadal oscillation and the Indian summer monsoon in CMIP5 models. Clim Dyn 51:3023–3039. https://doi.org/10.1007/s00382-017-4062-6

Lyu K, Yu JY (2017) Climate impacts of the Atlantic Multidecadal Oscillation simulated in the CMIP5 models: A re-evaluation based on a revised index. Geophys Res Lett 44:3867–3876. https://doi.org/10.1002/2017GL072681

Malik A, Brönnimann S, Stickler A, et al (2017) Decadal to multi-decadal scale variability of Indian summer monsoon rainfall in the coupled ocean-atmosphere-chemistry climate model SOCOL-MPIOM. Clim Dyn 49:3551–3572. https://doi.org/10.1007/s00382-017-3529-9

Mantua NJ, Hare SR, Zhang Y, et al (1997) A Pacific Interdecadal Climate Oscillation with Impacts on Salmon Production. Bull Am Meteorol Soc 78:. https://doi.org/10.1175/1520-0477(1997)078<1069:APICOW>2.0.CO;2

Menon A, Levermann A, Schewe J, et al (2013) Consistent increase in Indian monsoon rainfall and its variability across CMIP-5 models. Earth Syst Dyn 4:287–300. https://doi.org/10.5194/esd-4-287-2013

Mooley DA, Parthasarathy B (1984) Fluctuations in All-India summer monsoon rainfall during 1871-1978. Clim Change 6:. https://doi.org/10.1007/BF00142477

Naidu PD, Ganeshram R, Bollasina MA, et al (2020) Coherent response of the Indian Monsoon Rainfall to Atlantic Multi-decadal Variability over the last 2000 years. Sci Rep 10:. https://doi.org/10.1038/s41598-020-58265-3

Parker D, Folland C, Scaife A, et al (2007) Decadal to multidecadal variability and the climate change background. J Geophys Res Atmos 112:1–18. https://doi.org/10.1029/2007JD008411

Parzen E (1962) On Estimation of a Probability Density Function and Mode. Ann Math Stat 33:. https://doi.org/10.1214/aoms/1177704472

Peings Y, Magnusdottir G (2014) Forcing of the wintertime atmospheric circulation by the multidecadal fluctuations of the North Atlantic ocean. Environ Res Lett 9:. https://doi.org/10.1088/1748-9326/9/3/034018

Peings Y, Simpkins G, Magnusdottir G (2016) Multidecadal fluctuations of the North Atlantic Ocean and feedback on the winter climate in CMIP5 control simulations. J Geophys Res Atmos 121:2571–2592. https://doi.org/10.1002/2015JD024107

Rayner NA, Parker DE, Horton EB, et al (2003) Global analyses of sea surface temperature, sea ice, and night marine air temperature since the late nineteenth century. J Geophys Res Atmos 108:. https://doi.org/10.1029/2002jd002670

Rosenblatt M (1956) Remarks on Some Nonparametric Estimates of a Density Function. Ann Math Stat 27:. https://doi.org/10.1214/aoms/1177728190

Roy I, Kripalani RH (2019) The role of natural factors (part 2): Indian summer monsoon in climate change period—observation and CMIP5 models. Theor Appl Climatol. https://doi.org/10.1007/s00704-019-02864-2

Sabeerali CT, Rao SA, Dhakate AR, et al (2015) Why ensemble mean projection of south Asian monsoon rainfall by CMIP5 models is not reliable? Clim Dyn 45:. https://doi.org/10.1007/s00382-014-2269-3

Sandeep N, Swapna P, Krishnan R, et al (2022) On the weakening association between South Asian Monsoon and Atlantic Multidecadal Oscillation. Clim Dyn. https://doi.org/10.1007/s00382-022-06224-1

Sankar S, Svendsen L, Gokulapalan B, et al (2016) The relationship between Indian summer monsoon rainfall and Atlantic multidecadal variability over the last 500 years. Tellus, Ser A Dyn Meteorol Oceanogr 68:. https://doi.org/10.3402/tellusa.v68.31717

Schlesinger ME, Ramankutty N (1994) An oscillation in the global climate system of period 65–70 years. Nature 367:723–726. https://doi.org/10.1038/367723a0

Schmidt GA, Jungclaus JH, Ammann CM, et al (2012) Climate forcing reconstructions for use in PMIP simulations of the Last Millennium (v1.1). Geosci Model Dev 5:185–191. https://doi.org/10.5194/gmd-5-185-2012

Sengupta A, Rajeevan M (2013) Uncertainty quantification and reliability analysis of CMIP5 projections for the Indian summer monsoon. Curr Sci 105:1692–1703

Sinha A, Berkelhammer M, Stott L, et al (2011) The leading mode of Indian Summer Monsoon precipitation variability during the last millennium. Geophys Res Lett 38:. https://doi.org/10.1029/2011GL047713

Sinha A, Cannariato KG, Stott LD, et al (2007) A 900-year (600 to 1500 A.D.) record of the Indian summer monsoon precipitation from the core monsoon zone of India. Geophys Res Lett 34:. https://doi.org/10.1029/2007GL030431

Srivastava AK, Rajeevan M, Kulkarni R (2002) Teleconnection of OLR and SST anomalies over Atlantic Ocean with Indian summer monsoon. Geophys Res Lett 29:125-1-125–4. https://doi.org/10.1029/2001gl013837

Sun C, Kucharski F, Li J, et al (2017) Western tropical Pacific multidecadal variability forced by the Atlantic multidecadal oscillation. Nat Commun 8:1–10. https://doi.org/10.1038/ncomms15998

Sun C, Li J, Kucharski F, et al (2019) Recent Acceleration of Arabian Sea Warming Induced by the Atlantic-Western Pacific Trans-basin Multidecadal Variability. Geophys Res Lett 46:1662–1671. https://doi.org/10.1029/2018GL081175

Tejavath CT, Ashok K, Chakraborty S, Ramesh R (2019) A PMIP3 narrative of modulation of ENSO teleconnections to the Indian summer monsoon by background changes in the Last Millennium. Clim Dyn 53:. https://doi.org/10.1007/s00382-019-04718-z

Ting M, Kushnir Y, Seager R, Li C (2011) Robust features of Atlantic multi-decadal variability and its climate impacts. Geophys Res Lett 38:1–6. https://doi.org/10.1029/2011GL048712

Trenberth KE, Shea DJ (2006) Atlantic hurricanes and natural variability in 2005. Geophys Res Lett 33:. https://doi.org/10.1029/2006GL026894

Tung KK, Zhou J (2013) Using data to attribute episodes of warming and cooling in instrumental records. Proc Natl Acad Sci U S A 110:2058–2063. https://doi.org/10.1073/pnas.1212471110

Wang Y, Li S, Lu D (2009) Seasonal response of Asian monsoonal climate to the Atlantic

Multidecadal Oscillation. J Geophys Res Atmos 114:. https://doi.org/10.1029/2008JD010929

Wang X, Li J, Sun C, Liu T (2017) NAO and its relationship with the Northern Hemisphere mean surface temperature in CMIP5 simulations. J Geophys Res 122:. https://doi.org/10.1002/2016JD025979

Webster PJ, Yang S (1992) Monsoon and Enso: Selectively Interactive Systems. Q J R Meteorol Soc 118:. https://doi.org/10.1002/qj.49711850705

Welch P (1967) The use of fast Fourier transform for the estimation of power spectra: A method based on time averaging over short, modified periodograms. IEEE Trans Audio Electroacoust 15:70–73. https://doi.org/10.1109/TAU.1967.1161901

Wu B, Lin J, Zhou T (2016) Interdecadal circumglobal teleconnection pattern during boreal summer. Atmos Sci Lett 17:446–452. https://doi.org/10.1002/asl.677

Wu L, Liu Z (2005) North Atlantic decadal variability: Air-sea coupling, oceanic memory, and potential Northern Hemisphere resonance. J Clim 18:. https://doi.org/10.1175/JCLI-3264.1

Xavier PK, Marzin C, Goswami BN (2007) An objective definition of the Indian summer monsoon season and a new perspective on the ENSO-monsoon relationship. Q J R Meteorol Soc 133:. https://doi.org/10.1002/qj.45

Yang YM, An S Il, Wang B, Park JH (2020) A global-scale multidecadal variability driven by Atlantic multidecadal oscillation. Natl Sci Rev 7:. https://doi.org/10.1093/nsr/nwz216

Zhang R, Delworth TL (2006) Impact of Atlantic multidecadal oscillations on India/Sahel rainfall and Atlantic hurricanes. Geophys Res Lett 33:. https://doi.org/10.1029/2006GL026267

Zhang R, Delworth TL (2007) Impact of the Atlantic Multidecadal Oscillation on North Pacific climate variability. Geophys Res Lett 34:2–7. https://doi.org/10.1029/2007GL031601

Zhou T, Brönnimann S, Griesser T, et al (2010) A reconstructed dynamic Indian monsoon index extended back to 1880. Clim Dyn 34:. https://doi.org/10.1007/s00382-009-0552-5

Statements & Declarations

Funding

AD acknowledges the INSPIRE research fellowship from Department of Science and Technology, Government of India, for funding his doctoral research work. NJM acknowledges the DST Climate Change grant for funding her research.

Author Contributions

NJM perceived the idea and AD and RS carried out the analysis. All the authors contributed to the writing and presentation of the manuscript.

Competing Interests

The authors have no relevant financial or non-financial interests to disclose.

Data Availability

All original data sets used in the study are publicly available and the details are provided in the Data and Methodology section.

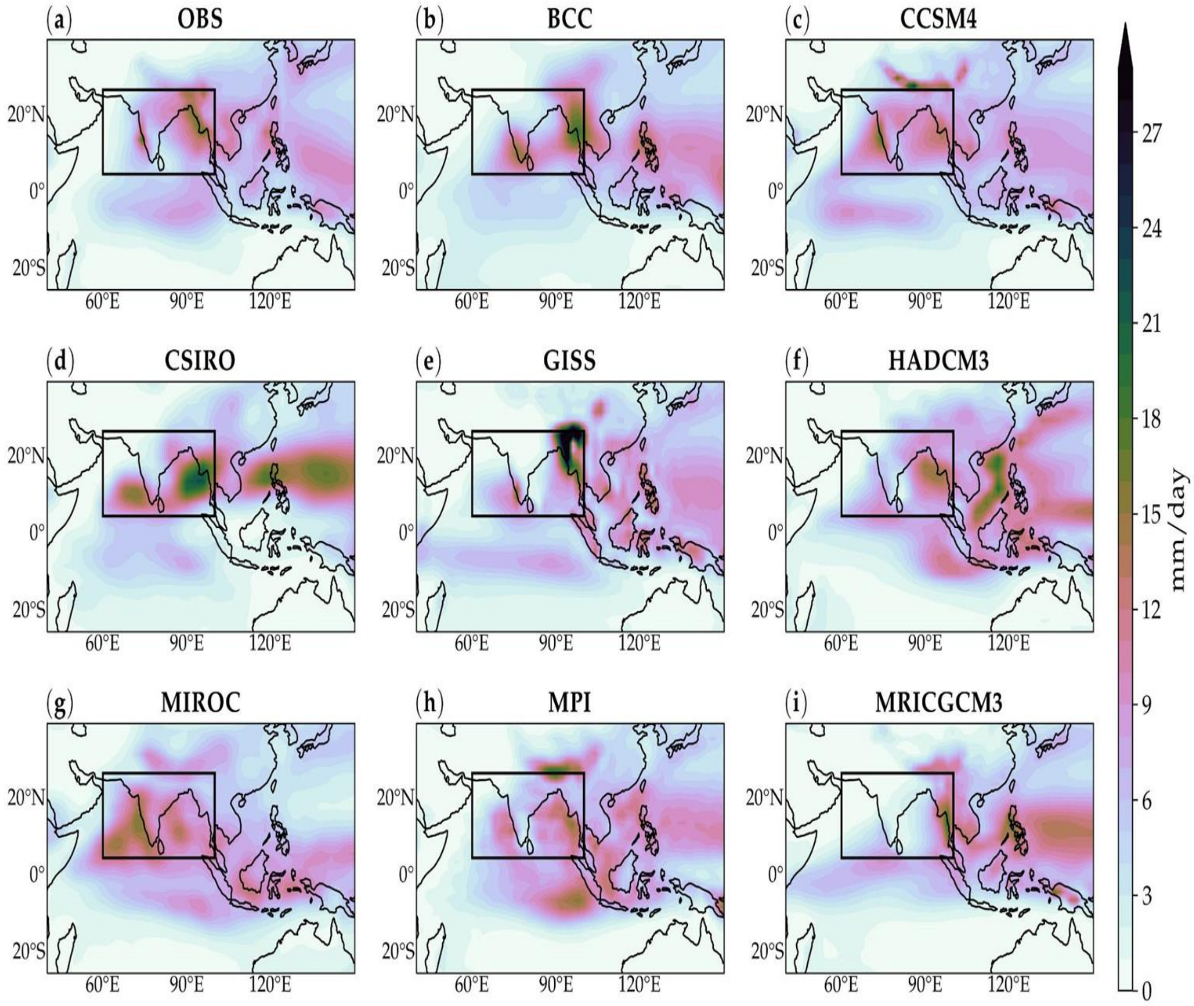

Figure 1: June to September (JJAS) mean monsoon rainfall in the (a) GPCP data (1979-2012) and (b)-(i) PMIP3 models LM simulations from 850-1850 AD.

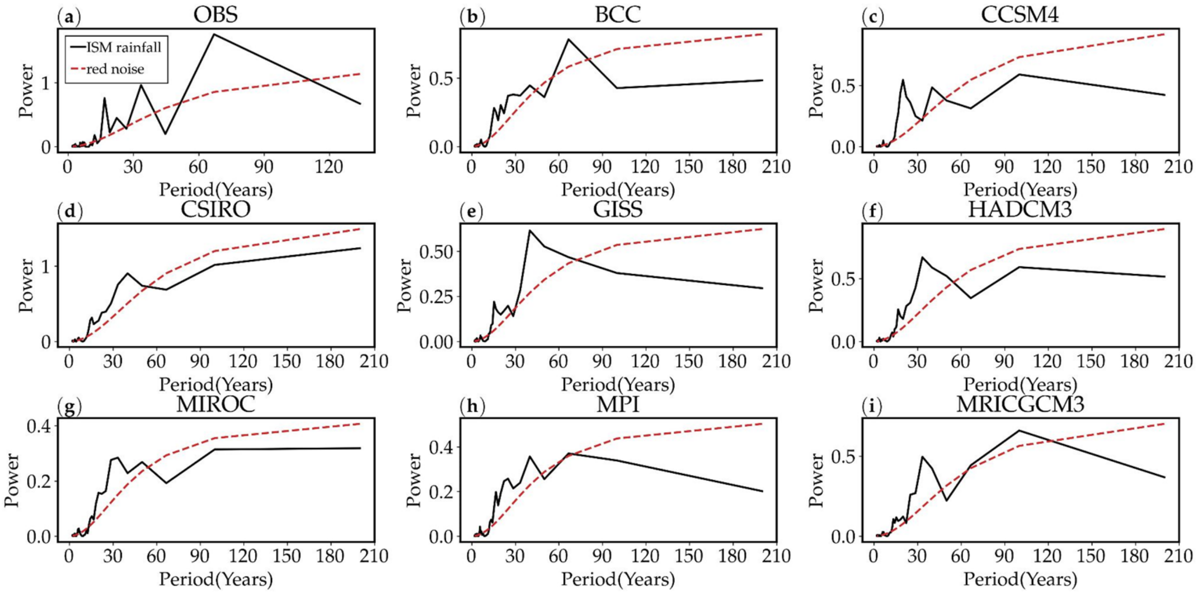

Figure 2: Power spectra of (a) IITM all-India mean ISM rainfall data (1871-2012) and (b)-(i) JJAS mean ISM rainfall averaged over 60°-100°E, 5°-27°N in the PMIP3 models LM simulations from 850-1850 AD. Red dashed line represents the red noise spectra.

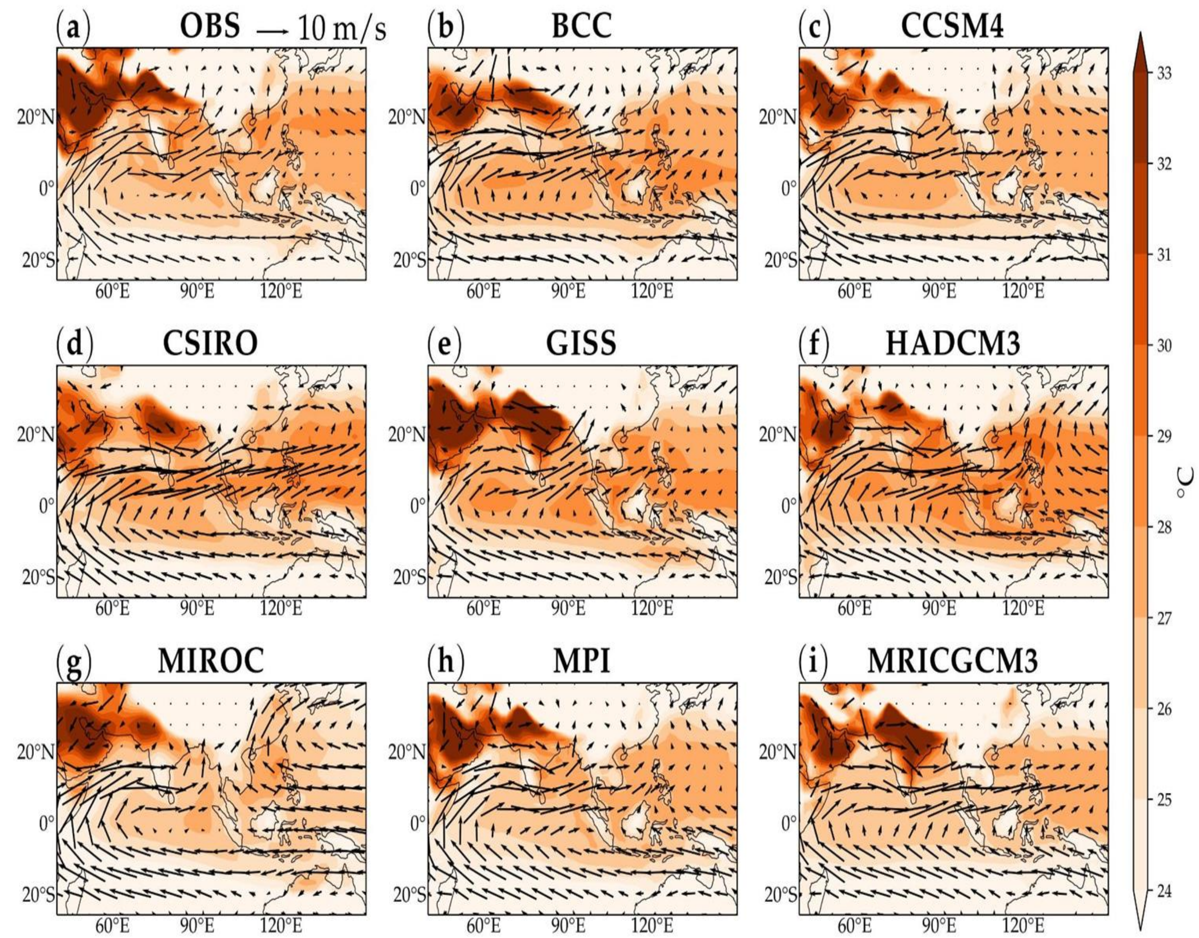

Figure 3: JJAS mean 850 hPa winds (vectors) and surface air temperature (shaded) in (a) 20th Century reanalysis V2 (1901-2012) and (b)-(i) PMIP3 models LM simulations from 850-1850 AD.

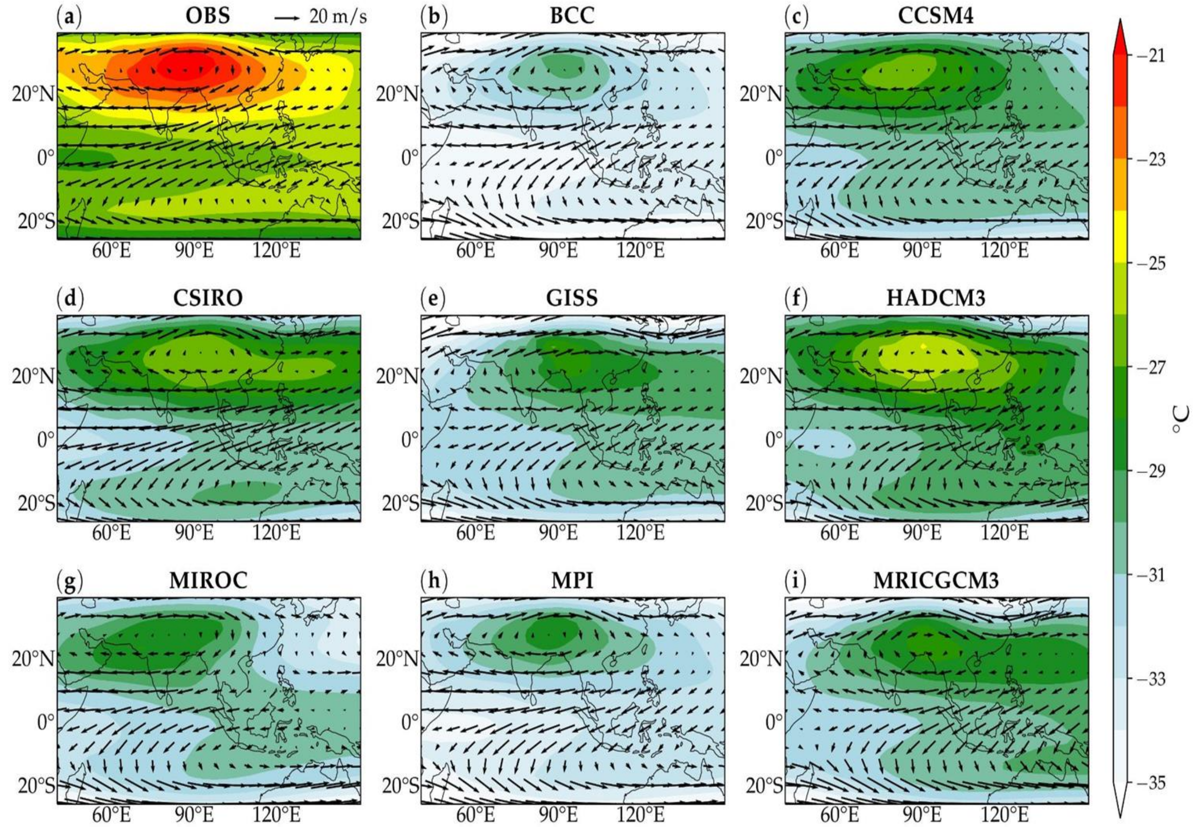

Figure 4: JJAS mean 200 hPa winds (vectors) and free tropospheric temperature (500-200 hPa) in (a) 20th Century reanalysis V2 (1901-2012) and (b)-(i) PMIP3 models LM simulations from 850-1850 AD.

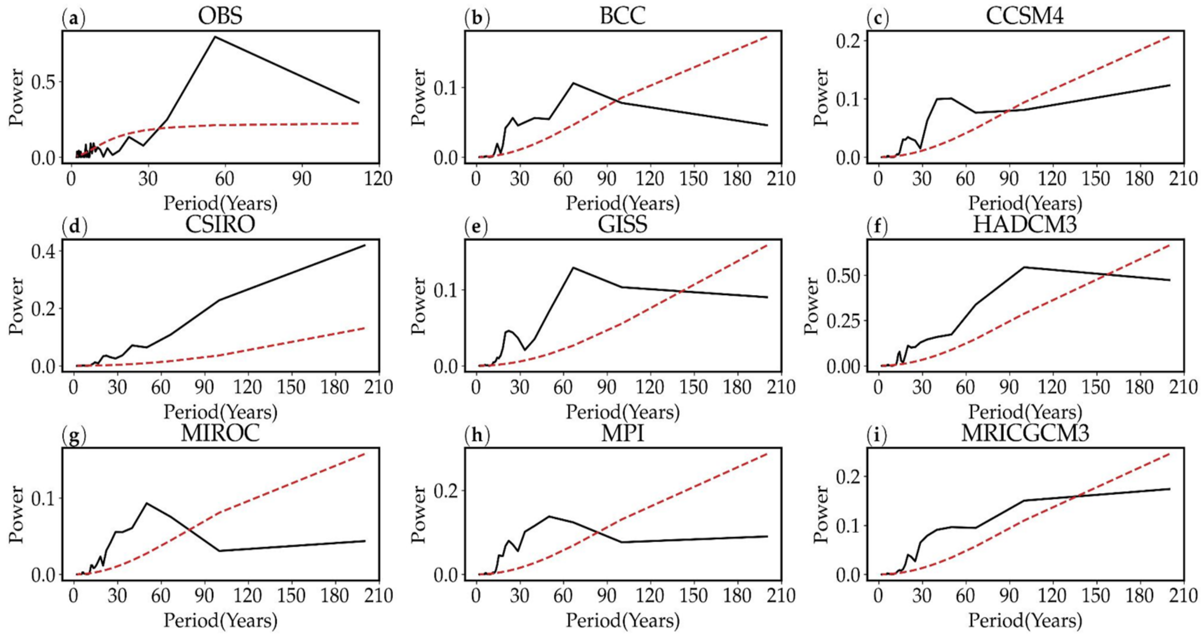

Figure 5: Power spectra of north Atlantic SST area averaged over (75°W -5°E, 0-60°N) in (a) HADISST (from 1901-2012) and (b)-(i) PMIP3 models LM simulations from 850-1850 AD. Red dashed line represents the red noise spectra.

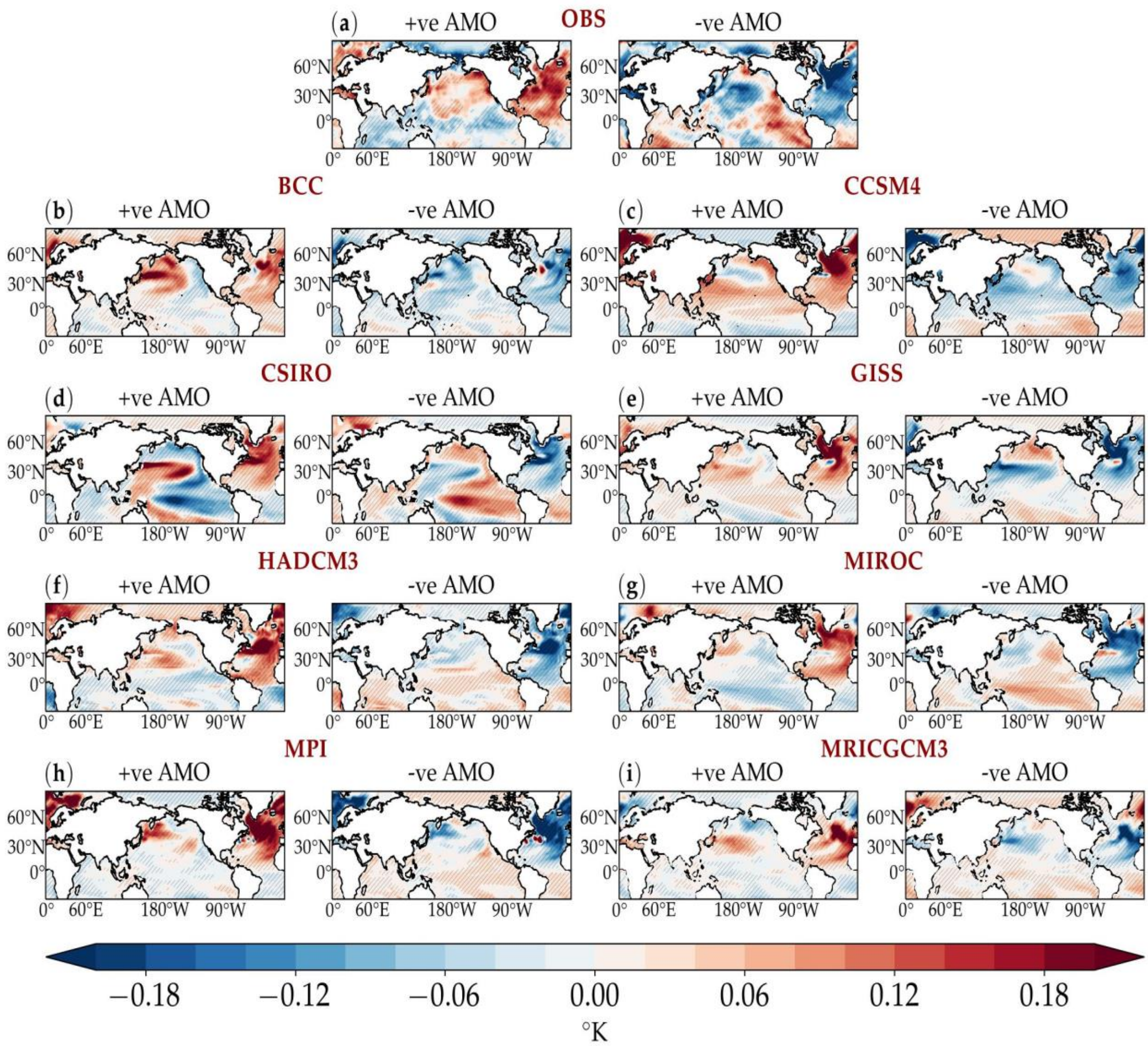

Figure 6: 30-100 year filtered, SST anomalies composited for positive and negative phases of AMO in (a) HADISST and (b)-(i) PMIP3 models LM simulations.

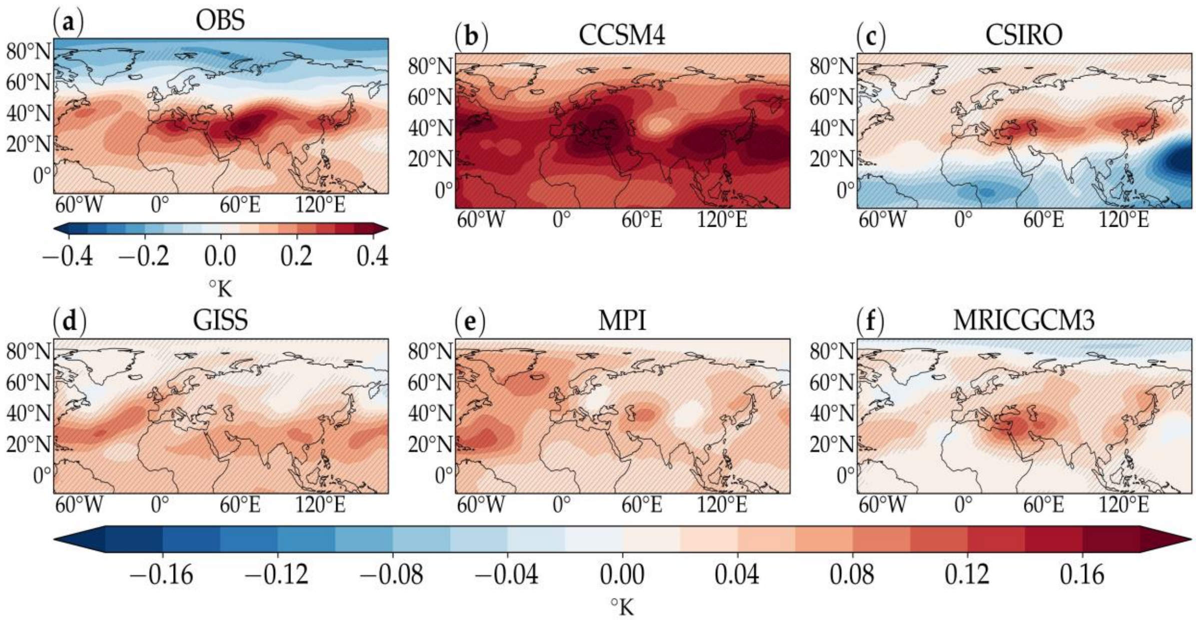

Figure 7: 30-100 year filtered free tropospheric temperature anomalies composited for the positive phase of AMO in (a) 20th Century reanalysis and (b)-(f) PMIP3 models LM simulations. Hatched regions represent statistical significance at 90% level.

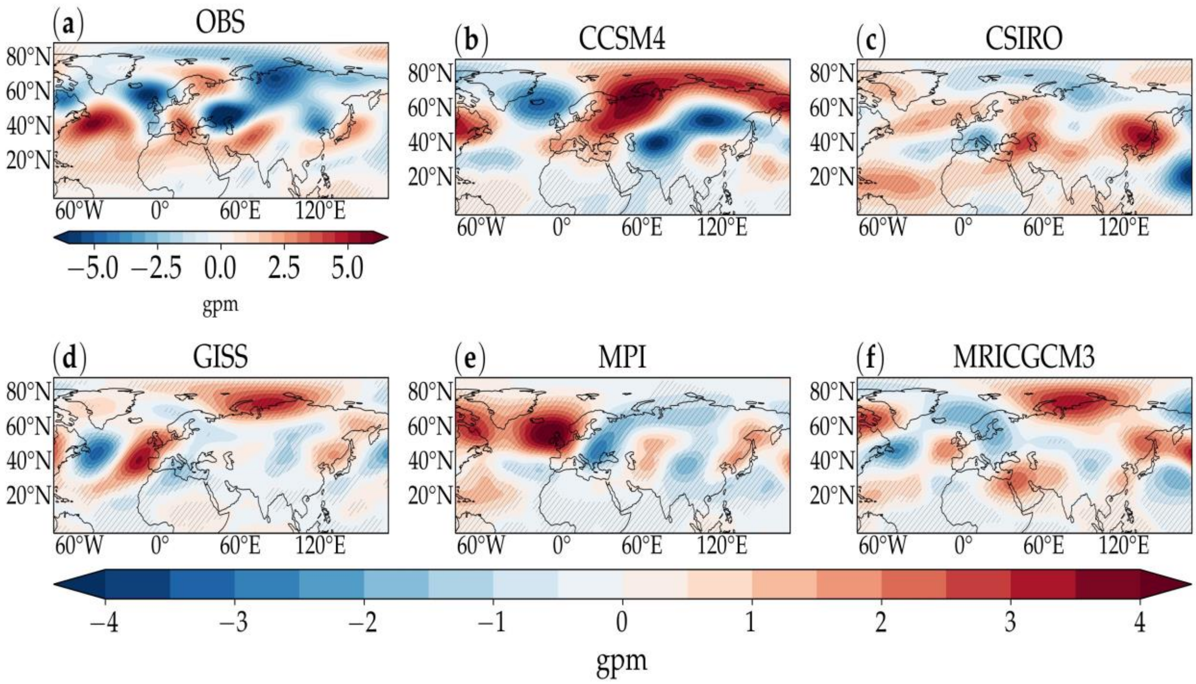

Figure 8: 30-100 year filtered 200 hPa eddy geopotential height anomalies composited for the positive phase of AMO in (a) 20th Century reanalysis and (b)-(f) PMIP3 models LM simulations. Hatched regions represent statistical significance at 90% level.

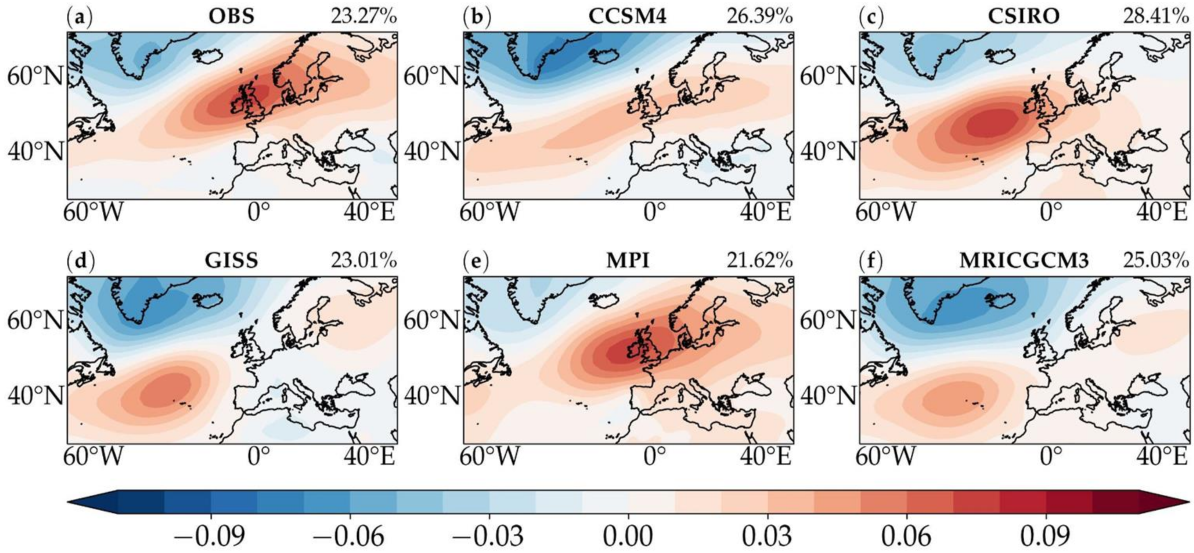

Figure 9: Summer NAO pattern in (a) 20th Century reanalysis and (b)-(f) PMIP3 models LM simulations. SNAO pattern is identified as the leading EOF of Jul-Aug Sea Level Pressure over the North Atlantic domain (70°W-50°E, 25°N-70°N). Variance explained by the mode is indicated as percentages.

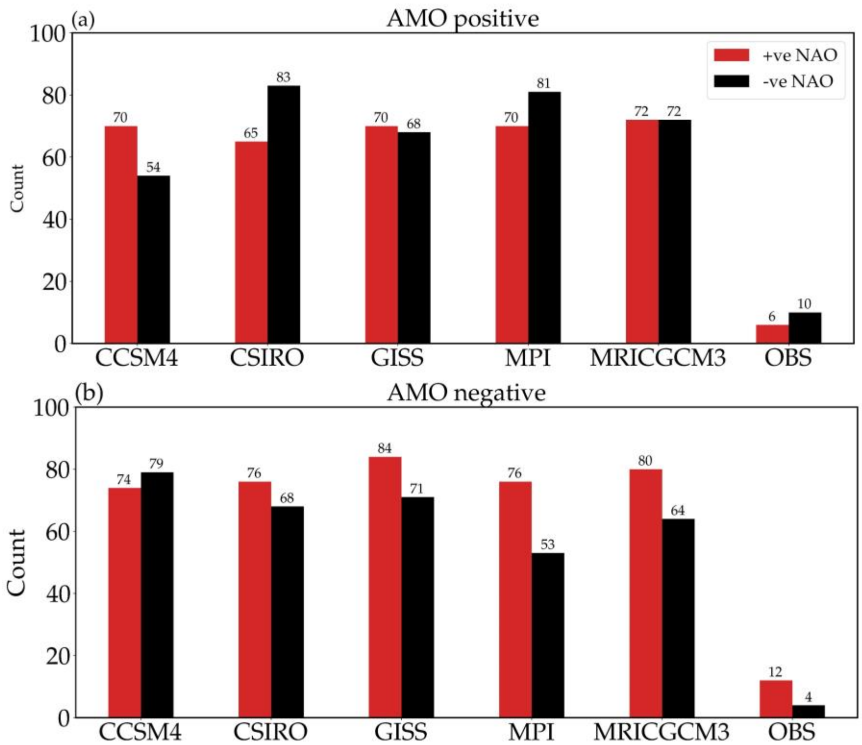

Figure 10: Frequency of occurrence of summer NAO in the positive and negative phases during a) AMO positive phase b) AMO negative phase in observations and PMIP3 models LM simulations.

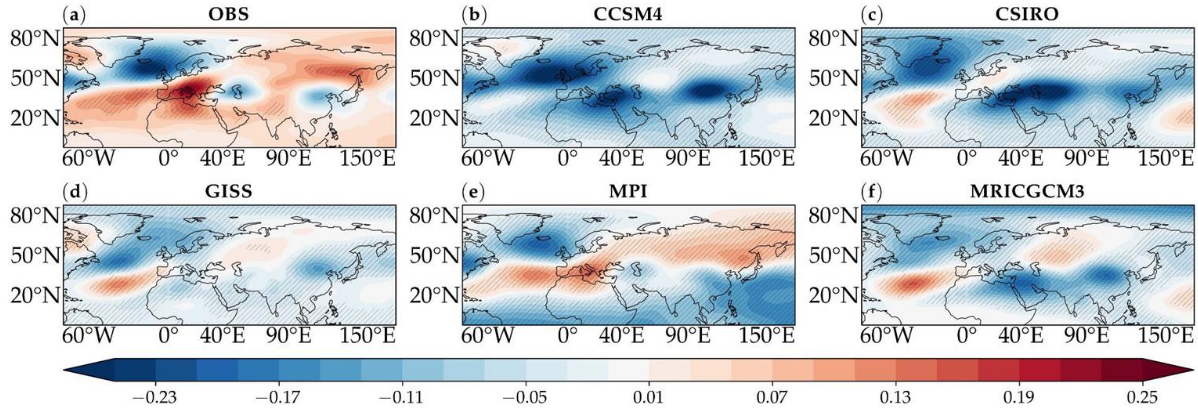

Fig 11: Regression coefficients obtained when unfiltered JJAS tropospheric temperature (500-200mb) anomalies are regressed onto the SNAO index in (a) 20th Century reanalysis and (b)-(f) PMIP3 models LM simulations. The regression coefficients are multiplied by -1 to represent the state corresponding to negative SNAO. Hatched regions represent statistical significance at 90% level.

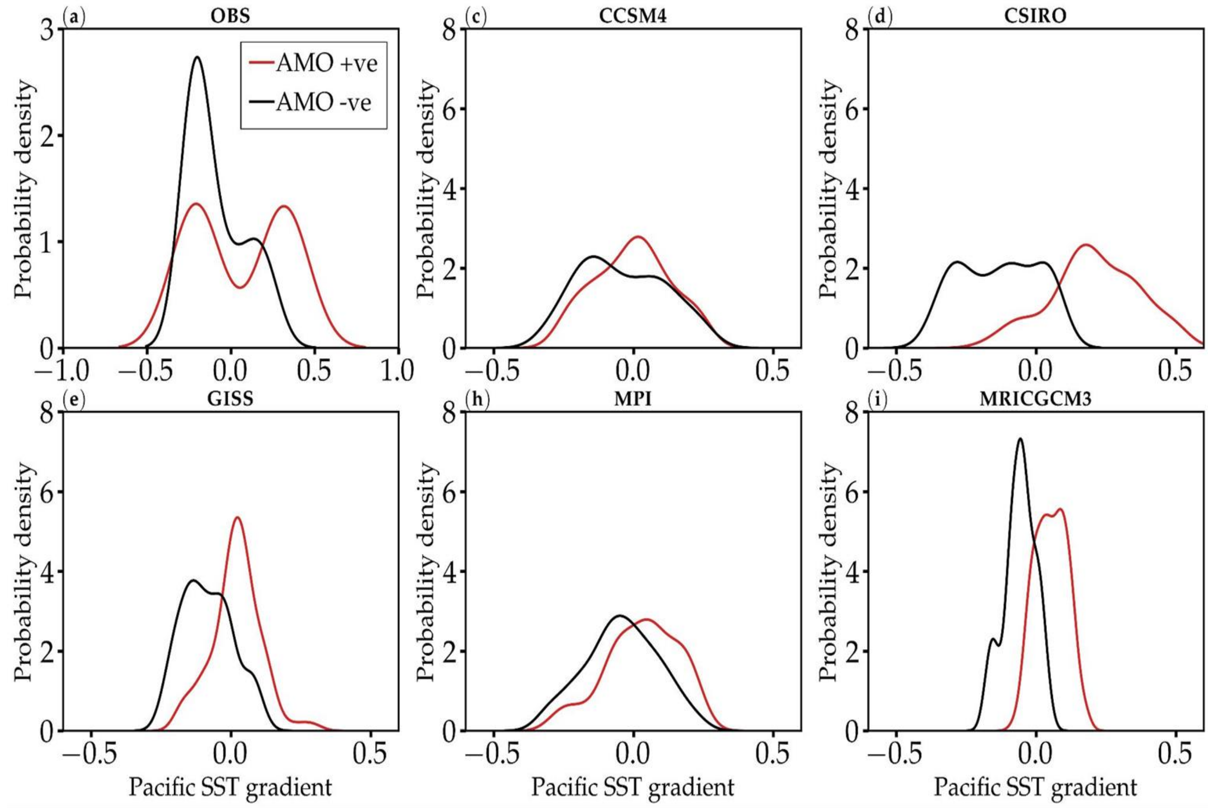

Figure 12: Probability distribution of 30-100 year filtered extratropical-tropical gradient values over the Pacific during positive and negative AMO phases in (a) HADISST and (b)-(i) PMIP3 models LM simulations. SST gradient is defined as the difference between area averaged SST anomalies over the north Pacific (25°-45°N, 150°E–140°W) and equatorial east Pacific (15°S-15°N, 180°-95°W).

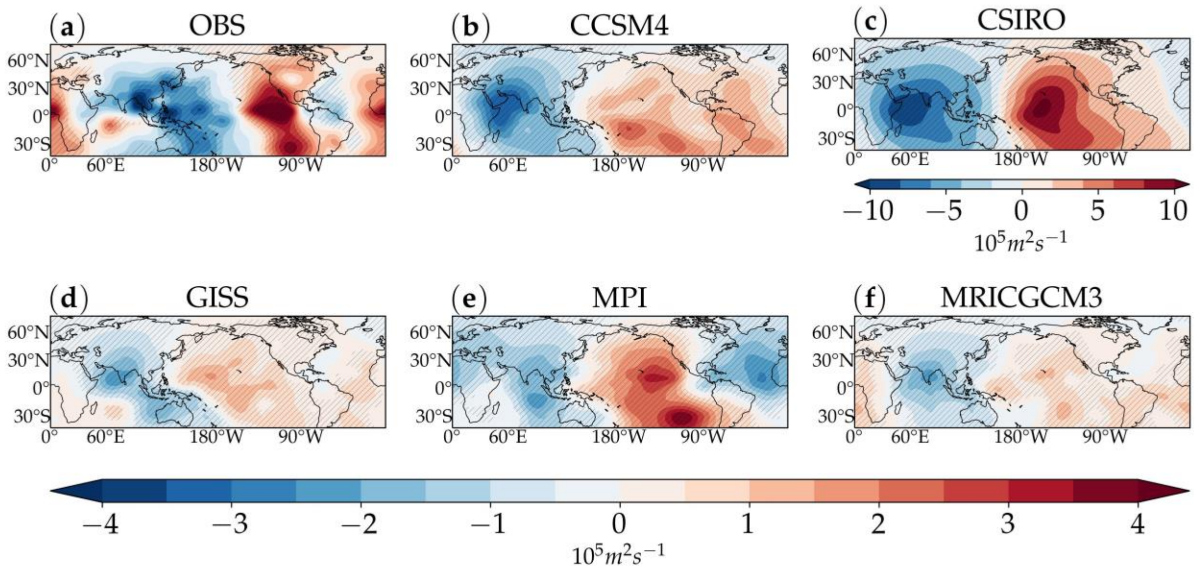

Figure 13: 30-100 year filtered 200 hPa velocity potential anomalies composited for the periods when the 30-100 year filtered extratropical-tropical gradient index values were positive over the Pacific, in (a) 20th Century reanalysis and (b)-(f) PMIP3 models LM simulations.

Model abbreviation	Model/Institute	Resolution
BCC-CSM-1	Beijing Climate Center, Climate system model version 1.1	T42, 26 levels
CCSM4	Community Climate System Model version 4, NCAR	1.25° × 0.942°, 26 levels
CSIRO-Mk3L-1-2	Commonwealth Scientific and Industrial Research organization Mark version 3.6.0	T21, 18 levels
GISS-E2-R	NASA Goddard Institute for Space Studies	2.5° × 2.0°, 40 levels
HadCM3	Hadley Centre Coupled Model version 3	3.75° × 2.5°, 19 levels
MIROC-ESM	University of Tokyo National Institute for Environmental Studies & JAMSTEC	T42, 80 levels
MPI-ESM-P	Max Plank Institute of Meteorology	T63, 47 levels
MRI-CGCM3	Meteorological Research Institute Japan	T102, 48 levels

Table 1 List of PMIP3 models analysed in the study.

	AMO-ISM (rainfall)	**AMO-ISM (TT gradient; Goswami and Xavier, 2005)**	**AMO-ISM (easterly shear; Webster and Yang, 1992)**
Observation	0.59	0.80	-0.49
BCC	0.15	0.02*	-0.09*
CCSM4	0.48	0.34	-0.34
CSIRO	0.34	0.31	-0.27
GISS	0.08	0.18	-0.33
HADCM3	0.14*	-0.06*	-0.06*
MIROC	-0.26	-0.15	0.04*
MPI	0.02*	0.22	-0.31
MRICGCM3	0.35	0.31	-0.34

Table 2 Correlation between the AMO index and rainfall based, TT gradient based and easterly wind shear based ISM indices in observations and PMIP3 models LM simulations

	AMO-NAO	**AMO-Pacific SST gradient**
Observation	-0.38	0.27
CCSM4	0.31	0.15
CSIRO	-0.23	0.49
GISS	-0.19	0.29
MPI	-0.38	0.21
MRICGCM3	-0.15	0.46

Table 3 Correlation of the AMO index with the 30-100 years filtered SNAO index and 30-100 years filtered extratropical-tropical SST gradient over the Pacific, in observations and PMIP3 models LM simulations. Principal components corresponding to the EOF modes shown in Figure 9 represent the SNAO indices. SST gradient is defined as the difference between area averaged SST anomalies over the north Pacific (25°-45°N, 150°E–140°W) and equatorial east Pacific (15°S-15°N, 180°E–95°W)